Chapter 2

Computer Codes and their Implementation

Abstract

Our understanding about Gamma Ray Bursts was revolutionised with the discovery of afterglows in 1997. The multiband observations of GRB afterglows led to discovering a variety of phenomenon associated with the GRBs, Fireball evolution, environments, and energetics. The multiband observations, even after a decade of their discovery, continue to reveal important information about the GRBs and throw up newer and newer problems. Modeling of multiband observations is guided by the fireball model but deviations from the expected behaviour also show up and are explained by certain assumptions.

In this chapter, we try to emphasize the importance of multiband observations. Also, we describe in detail the computer codes we built to test the predictions of the fireball model against the multiband observations of GRB afterglows.

2.1 Introduction

Most of our understanding about the GRBs, their origin, evolution, locations in the universe and energetics is tested and accumulated within last ten years thanks to the discovery of GRB afterglows in 1997. The models for the origin and evolution of GRBs were in the literature even before 1997 but it was only after the discovery of the afterglows that those could be tested. Thus, multiband observations of GRB afterglows are important for testing various models regarding the GRBs and their structure and evolution.

In Section § 2.2 of this Chapter we discuss the importance of multiband observations of GRB afterglows. We built a few computer codes to compare the observations with model predictions. We describe these codes and their implementation in detail in Section § 2.3.

2.2 Importance of Multiband Observations and Modeling

We have come across the physical parameters of GRB fireballs : E, n (or A), p, ϵ_e and ϵ_B. All these unknown physical parameters are connected to four different spectral observables viz. ν_a, ν_m, ν_c and F_{ν_m}. The value of p can be deduced from the observed spectral and temporal slopes of the light curves i.e. from α and β. Thus, if all the observables could be fixed from observations, one can deduce all the physical parameters about the explosion. Since, the concerned spectral observables are expected to lie in different wavelength regions viz. x-ray, optical and radio, simultaneous observations of afterglows in all these wavebands are very important. We have estimated physical parameters of a few GRBs by using their spectral parameters obtained from observations. For details, please see Chapters in this thesis about

GRB 030329, GRB 050401 and GRB 050319.

Multifrequency observations are also important to infer the existence of breaks in the afterglow light curves and further to determine the chromaticity or achromaticity of the breaks. This information about breaks is very important to know if the cause of the break is dynamical or spectral. In the case of GRB 030329, a smooth achromatic break in its radio light curve is seen. This has been attributed to the transition of the shock wave from relativistic to non-relativistic expansion. See e.g. Frail et al. (2005a); Resmi et al. (2005) and Chapter 4 of this thesis. In the study of GRB 050319, we inferred a presence of achromatic break from the multifrequncy light curves of GRB 050319. This afterglow is explained in Chapter 6 using a model which assumes transition of the circum-burst medium from wind density to the constant density profile. In an interesting case of GRB 050401, a break in the x-ray light curve is see which is not accompanied by similar break in the optical light curve. In Chapter 5, we have modeled this afterglow light curve using a model in which two co-axial jets are powering the afterglows at different wavebands. Thus the multifrequncy observations of the afterglow are among the most important tools to study the GRB, its evolution and about its surroundings.

2.3 Codes for Fitting the Multiband Afterglows

During the course of this thesis, we have tried to estimate various physical parameters (E, n (or A), p, ϵ_e and ϵ_B) of GRBs and afterglows using multifrequency observations of the afterglows and by comparing them with various physical models. For this purpose we have built computer codes which can use the observations, compare them with prescribed models and return the physical parameters. Below we describe briefly these codes and various computations they perform.

	Homogeneous Density Medium $[n(r) \propto r^0]$		Wind Density Medium $[n(r) \propto r^{-2}]$	
	$t < t_j$	$t > t_j$	$t < t_j$	$t > t_j$
$\nu < \nu_a < \nu_c < \nu_m$	$\nu^2 t^1$	$\nu^2 t^1$	$\nu^2 t^2$	$\nu^2 t^1$
$\nu_a < \nu < \nu_c < \nu_m$	$\nu^{1/3} t^{1/6}$	$\nu^{1/3} t^{-1}$	$\nu^{1/3} t^{-2/3}$	$\nu^{1/3} t^{-1}$
$\nu_a < \nu_c < \nu < \nu_m$	$\nu^{-1/2} t^{-1/4}$	$\nu^{-1/2} t^{-1}$	$\nu^{-1/2} t^{-1/4}$	$\nu^{-1/2} t^{-1}$
$\nu_a < \nu_c < \nu_m < \nu$	$\nu^{-p/2} t^{-(3p-2)/4}$	$\nu^{-p/2} t^{-p}$	$\nu^{-p/2} t^{-(3p-2)/4}$	$\nu^{-p/2} t^{-p}$
$\nu < \nu_a < \nu_m < \nu_c$	$\nu^2 t^{1/2}$	$\nu^2 t^0$	$\nu^2 t^1$	$\nu^2 t^0$
$\nu_a < \nu < \nu_m < \nu_c$	$\nu^{1/3} t^{1/2}$	$\nu^{1/3} t^{-1/3}$	$\nu^{1/3} t^0$	$\nu^{1/3} t^{-1/3}$
$\nu_a < \nu_m < \nu < \nu_c$	$\nu^{-(p-1)/2} t^{-(3/4)(p-1)}$	$\nu^{-(p-1)/2} t^{-p}$	$\nu^{-(p-1)/2} t^{-(3p-1)/4}$	$\nu^{-(p-1)/2} t^{-p}$
$\nu_a < \nu_m < \nu_c < \nu$	$\nu^{-p/2} t^{-(3p-2)/4}$	$\nu^{-p/2} t^{-p}$	$\nu^{-p/2} t^{-(3p-2)/4}$	$\nu^{-p/2} t^{-p}$
$\nu < \nu_m < \nu_a < \nu_c$	$\nu^2 t^{1/2}$	$\nu^2 t^0$	$\nu^2 t^1$	$\nu^2 t^0$
$\nu_m < \nu < \nu_a < \nu_c$	$\nu^{5/2} t^{5/4}$	$\nu^{5/2} t^1$	$\nu^{5/2} t^{7/4}$	$\nu^{5/2} t^1$
$\nu_m < \nu_a < \nu < \nu_c$	$\nu^{-(p-1)/2} t^{-(3/4)(p-1)}$	$\nu^{-(p-1)/2} t^{-p}$	$\nu^{-(p-1)/2} t^{-(3p-1)/4}$	$\nu^{-(p-1)/2} t^{-p}$
$\nu_m < \nu_a < \nu_c < \nu$	$\nu^{-p/2} t^{-(3p-2)/4}$	$\nu^{-p/2} t^{-p}$	$\nu^{-p/2} t^{-(3p-2)/4}$	$\nu^{-p/2} t^{-p}$

Table 2.1: **Spectral and temporal scalings of GRB afterglow :** The various expected spectral regimes of GRB afterglows and position of the frequency of observations (ν) with respect to the various spectral breaks – ν_a, ν_m, ν_c are listed in column 1. Listed in columns 2 to 5 are the scalings of the afterglow evolution in the format $f_\nu \propto \nu^{-\beta}\ t^{-\alpha}$ where α and β are the spectral and temporal indices. The column 2 and column 4 refer to the afterglow evolution for homogeneous and wind medium density profiles respectively, before the jet break while the columns 3 and 5 refer to that after the jet break. All the parameters mentioned in the table are referred to the observer's frame of reference, though, for simplicity, we have dropped all the subscripts here.

Afterglow Radiation Models : The fireball model (Rees and Meszaros, 1992; Meszaros and Rees, 1993) is among the most popular models of GRBs and according to it the afterglow is due to synchrotron radiation from shocked relativistic electrons. Sari et al. (1998); Wijers and Galama (1999) and Chevalier and Li (2000) predict evolution of the afterglow spectrum and light curves for constant and wind density profiles of the CSM. The various spectral regimes and light curves as predicted by the fireball model are listed in Table 1. We have built subroutines which can calculate radiation from both kinds of density profiles of the CSM, constant and wind, at any given frequency of observation and at any given time.

Among the inputs to the codes are the break frequencies at any time. The codes then estimate the synchrotron flux expected from the afterglow at the epoch of observations by evolving the given spectral parameters to that particular epoch.

For illustration of the evolution of spectral breaks, ν_a, ν_m, ν_c, please see from Figure 2.1 to Figure 2.6.

Jet break and non-relativistic transition of the afterglow :

The standard fireball model, as mentioned above, have later on been added with various other effects such as the jet breaks due to collimated outflows and transition of the shock-wave to non-relativistic phase of evolution. We have generalised our codes by incorporating these modifications. Entire evolution of the spectrum and light curves can be calculated by specifying the guess values of the epochs of jet break (t_j) and non-relativistic transition (t_{NR}). The code can then return the best fit values of t_j and t_{NR} along with other parameters.

Smoothening of spectrum and light curves : The spectral and temporal breaks ex-

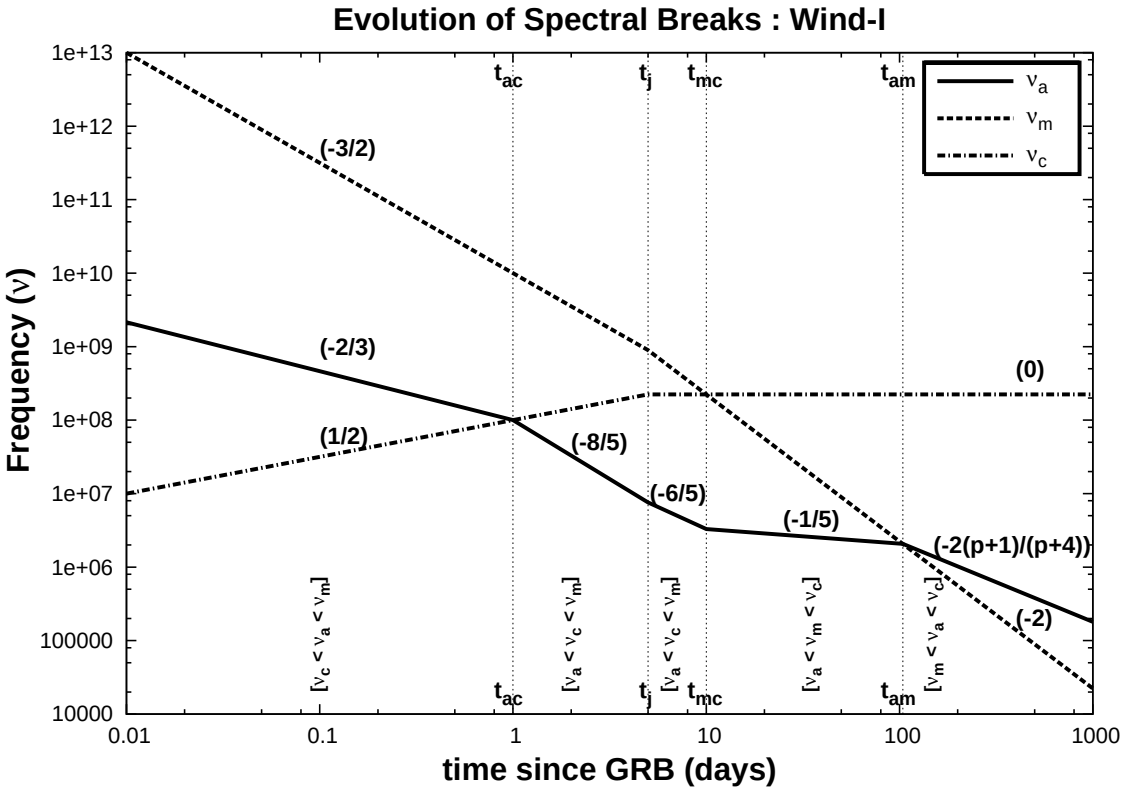

Figure 2.1: **The evolution of spectral breaks :** The plots show evolution of spectral breaks (ν_a, ν_m, ν_c) as predicted by the fireball model. Evolution due to a jet break is also taken into account. As the breaks evolve at different rates in time they cross each other at various epochs such as $t_{ac} \equiv t(\nu_a = \nu_c)$, $t_{mc} \equiv t(\nu_m = \nu_c)$ and $t_{am} \equiv t(\nu_a = \nu_m)$. The epoch of jet break is denoted by t_j. In the figure, these epochs are indicated by vertical dotted lines. The different relative arrangements of these epochs result due to different normalisations of spectral breaks at a given time which in turn are due to different physical conditions prevailing at the radiating ejecta. The spectral breaks evolve as a power law in time i.e. $\nu_b \propto t^q$ where ν_b is the spectral break and q is the index of power law. The numbers in the brackets on top of the lines representing the spectral breaks correspond to the index of their temporal evolution i.e. 'q'. The corresponding spectral regime is mentioned in the square brackets. This figure shows evolution of the spectral breaks due to the outflow expanding in the wind circum-burst density medium and considers a situation when $t_{ac} < t_j < t_{mc} < t_{am}$.

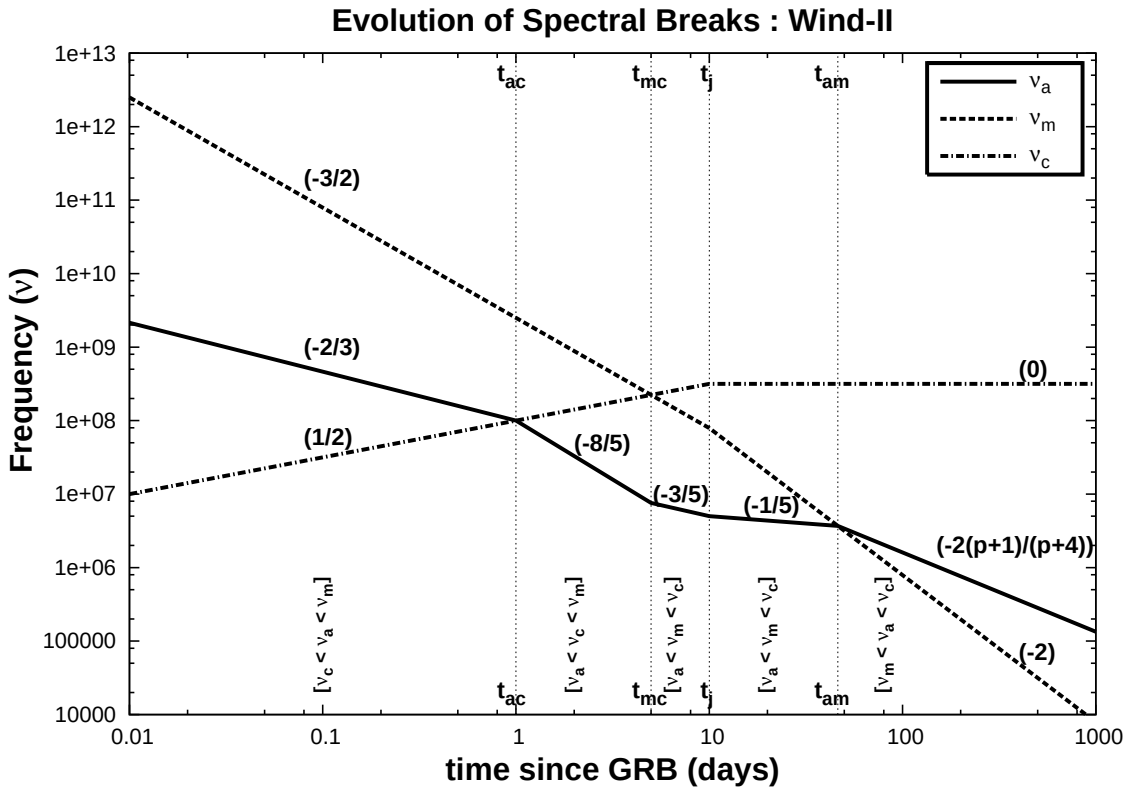

Figure 2.2: **The evolution of spectral breaks :** This figure is similar to Figure 2.1 but for $t_{ac} < t_{mc} < t_j < t_{am}$. For details please see the caption of Figure 2.1.

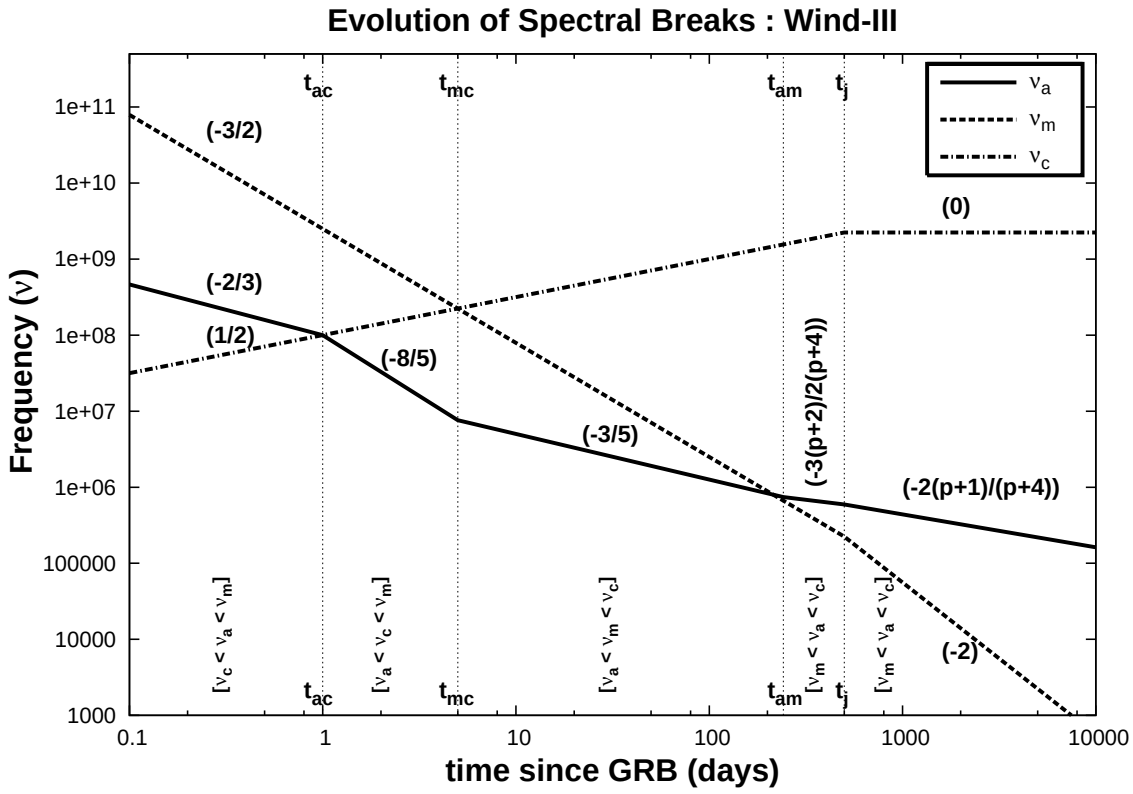

Figure 2.3: **The evolution of spectral breaks :** This figure is similar to Figure 2.1 but for $t_{ac} < t_{mc} < t_{am} < t_j$. For details please see the caption of Figure 2.1.

pected in the afterglow are never sharp. Because the observed radiation is integrated over a large radiating surface, all the spectral and temporal breaks have smooth evolution. To compare these smooth spectra and light curves with the model spectra and light curves they have to be smoothened appropriately. The detailed integration over the radiating surfaces is computationally expensive. Hence to achieve similar results to some extent we follow the smoothening prescription given by Granot and Sari (2002).

The spectra and light curves of afterglows show broken power law evolution. According to the Granot and Sari (2002) prescription, the flux density $F_{x,1}$ across a break can be described by joining two broken power laws at the break

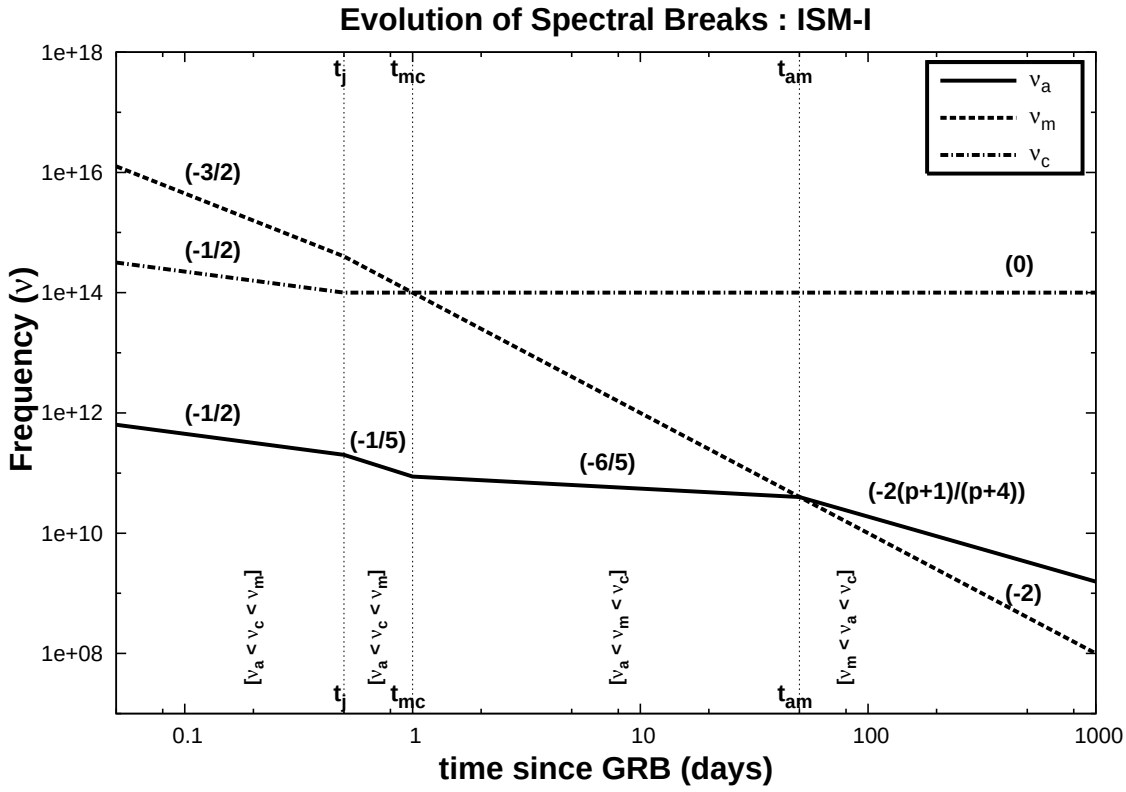

Figure 2.4: **The evolution of spectral breaks :** This figure is similar to Figure 2.1 but for homogeneous density profile of the CSM and for $t_j < t_{mc} < t_{am}$. For details please see the caption of Figure 2.1.

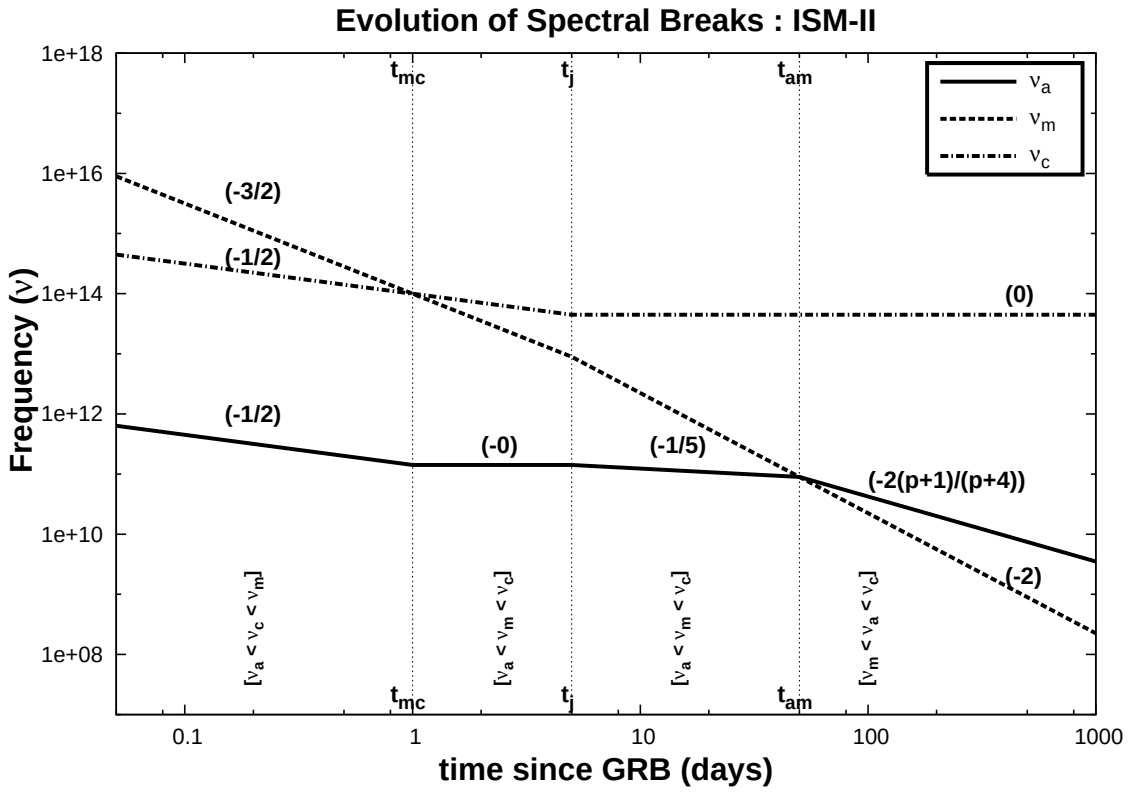

Figure 2.5: **The evolution of spectral breaks :** This figure is similar to Figure 2.4 but for $t_{mc} < t_j < t_{am}$. For details please see the caption of Figure 2.1.

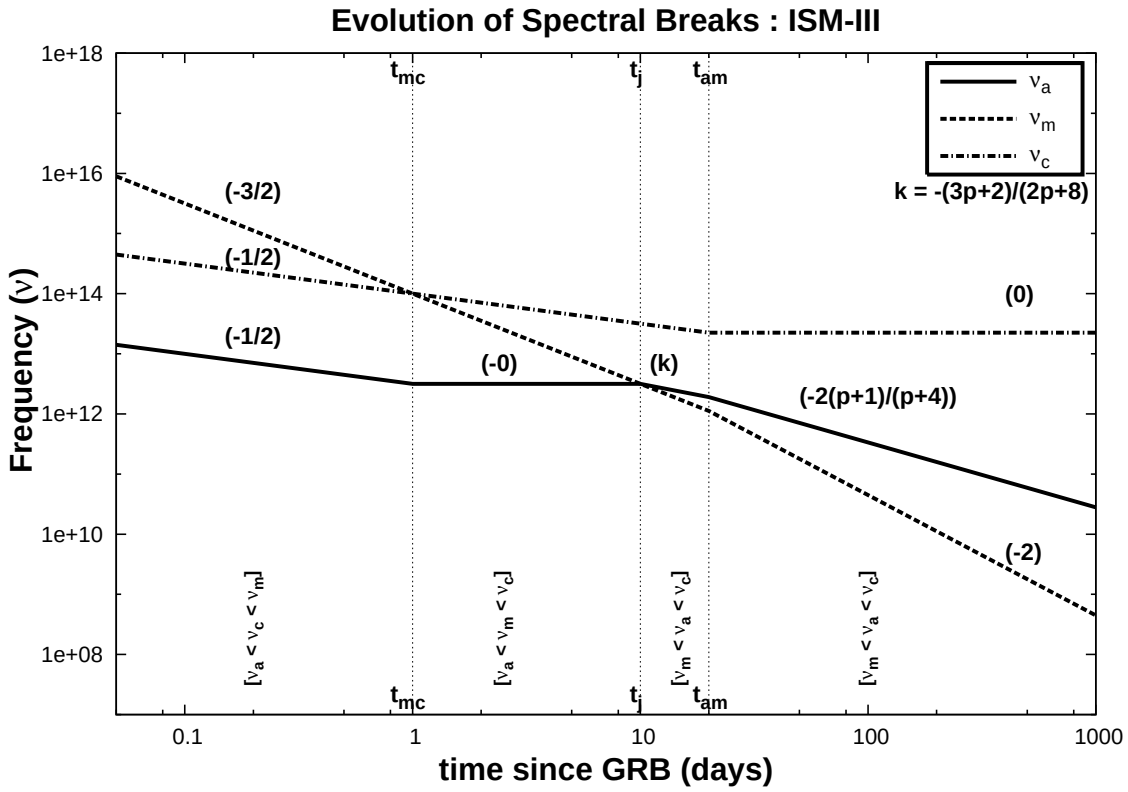

Figure 2.6: **The evolution of spectral breaks :** This figure is similar to Figure 2.4 but for $t_{mc} < t_{am} < t_j$. For details please see the caption of Figure 2.1.

point x_b :

$$F_{x,1} = F_{x,ext}\left[\left(\frac{x}{x_b}\right)^{-s_b q_1} + \left(\frac{x}{x_b}\right)^{-s_b q_2}\right]^{-1/s_b} \tag{2.1}$$

where x is time (t) or frequency ν depending on whether one is calculating a light curve or a spectrum, respectively, and q_1 and q_2 being the power law indices before and after the break point x_b. The smoothening parameter s_b has a sign similar to the sign of $(q_2 - q_1)$ i.e. s_b is +ve if the curve is steeping after the break. $F_{x,ext}$ corresponds to the normalisation of the flux in the absence of any smoothening. It may be noted that higher the numerical value of s_b, the sharper the break becomes. We use different smoothening parameters for smoothening the spectrum at different breaks viz. s_a, s_m, s_c, s_j, s corresponding to smoothening of spectral breaks ν_a, ν_m, ν_c, temporal break at t_j and a general smoothening of any other break (e.g. temporal breaks at various epochs crossing of spectral breaks), respectively. If the spectrum or light curve consists of more than one break, contributions from the subsequent power laws are estimated as

$$\tilde{F}_{x,2} = \left[1 + \left(\frac{x}{x_b}\right)^{s_b(q_1-q_2)}\right]^{1/s_b} \tag{2.2}$$

The final total flux is given by

$$F_x = F_{x,1} \times \tilde{F}_{x,2} \times .... \times \tilde{F}_{x,n} \tag{2.3}$$

where n corresponds to the number of power laws joined together.

Extinction in the host galaxy : The observed magnitudes and fluxes of the afterglow normally includes extinction along the line of sight, from the site of explosion to the observer. The intervening material is such that the extinction is maximum in optical and ultra-violet. Extinction law - frequency dependence of the extinction - for the Milky Way is given by by Mathis (1990) and the expected Galactic extinction in any given direction can be estimated using the

smoothed reddening map provided by Schlegel et al. (1998). A subroutine uses these estimates to correct the model flux for the galactic extinction.

Observations show that the host galaxies of GRBs are star-forming galaxies. During the light curve fitting, we found that the GRB host galaxy extinction is, on an average, better accounted for by the use of Calzetti's extinction law Calzetti et al. (1994). According to this law, the extinction can be approximated as a polynomial of wavelength λ. If $x = log_{10}(\lambda)$ and λ is given in units μm, then the extinction in magnitude at a wavelength λ, i.e. A_λ, is estimated using

$$A_\lambda = (0.9255 + x[-3.860 + x[1.631 + x[0.7363]]] + 0.2) \times E_{B-V_{host}} \qquad (2.4)$$

The best fit value of parameter $E_{B-V_{host}}$ is returned by the code.

Figure 2.7 shows a comparison between the Milky Way extinction law and Calzetti's extinction law.

Host galaxy contribution in the afterglow flux : The extinction in the afterglow flux reduces the brightness of the afterglow. But there is another component of contamination, which is present in most of the afterglow fluxes at different levels. This is the flux contribution of the GRB host galaxy itself. In some of the afterglows is manifests so much clearly that at late times the afterglow light curve remains at a constant brightness, which is of the level of the brightness of the host galaxy. The brightness of the host galaxy can be frequency dependent. If it is known directly from the host observations then a subroutine adds equivalent amount of flux in the model flux. Figure 2.8 shows sample optical light curves of GRB 991208 which clearly shows flattening due to the contribution from the host galaxy.

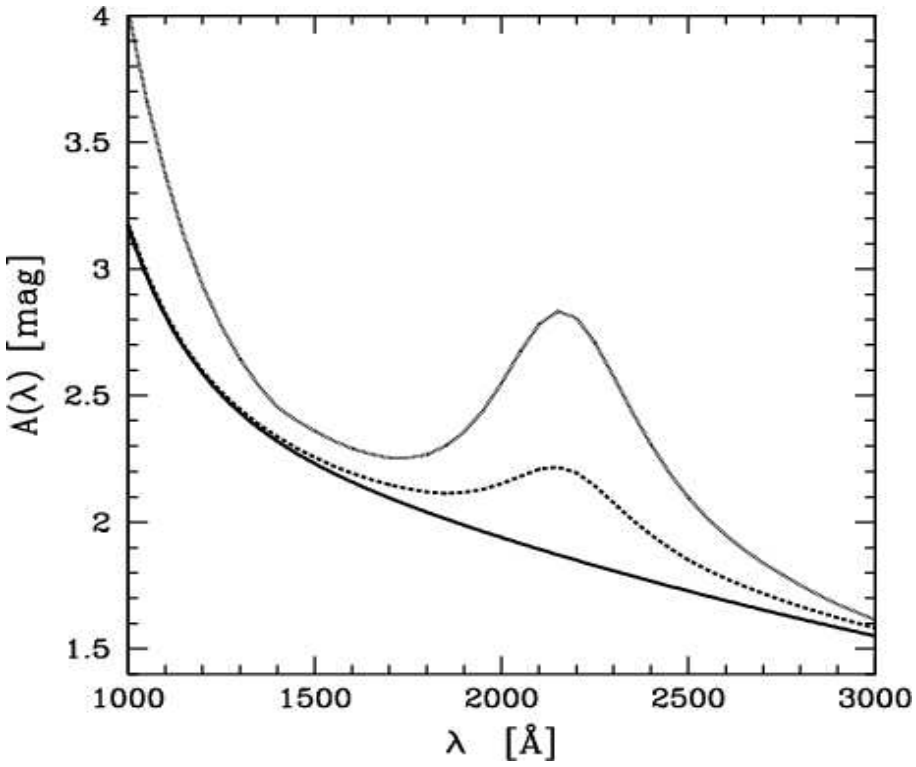

Figure 2.7: **Extinction laws :** Extinction (for E(B-V)=0.2) according to Calzetti's law (Calzetti et al., 1994)(solid black line), a superposition of Calzetti's law with 2175 Åbump (dashed line), and the extinction curve for the Milky Way (solid gray line). This figure is taken from Massarotti et al. (2001)

Data qualification and rejection : A sub-routine is built into the code to check the validity of the data points, weighted by their errors, by comparing with the model predictions. This gives a choice to accept or reject the data points that deviate from the model by not more than a certain level of significance. For example, user can specify if he/she wishes to consider only those data points for comparison with the model which does not deviate from the model beyond a certain level of significance, say $(n \times \sigma)$ where σ is the uncertainty associated with the measured flux and n can be user specified. All the data points which are beyond $n \times \sigma$ from the model predictions will then be rejected

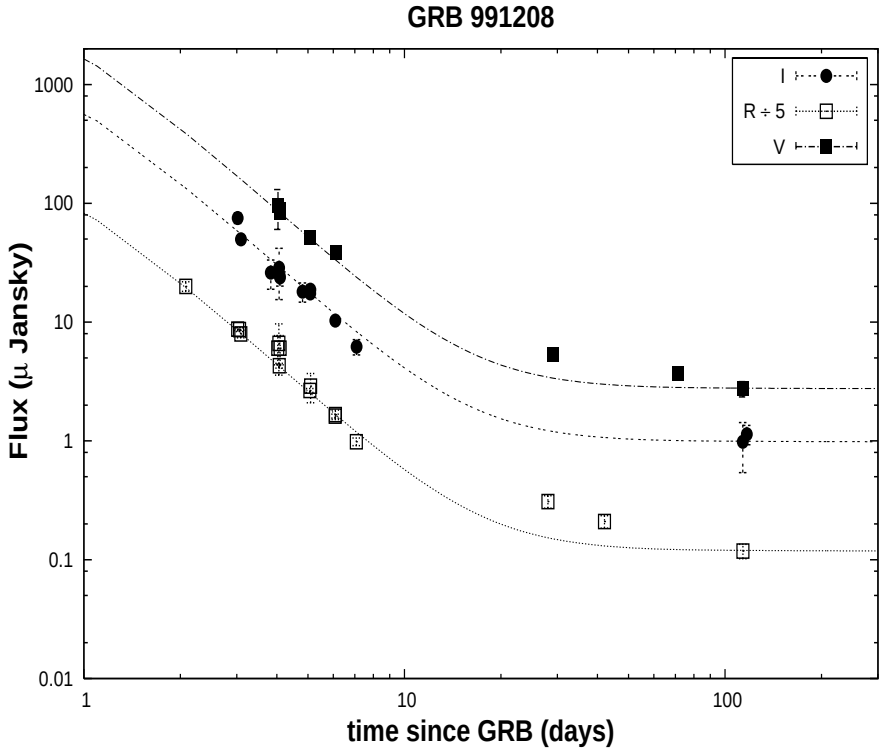

Figure 2.8: **Host Galaxy Contribution :** Flattening of the light curves of GRB 991208 afterglow due to contribution of the host galaxy light.

when compared with the model. This facility is particularly useful in the presence of a few large outliers in the dataset.

Statistics for model comparison : The statistics used as a measure of fit reliability is the χ^2 statistics. The code requires guess values of all the spectral breaks, peak flux at a given time, the electron distribution index (p) and also the guess values of jet break time (t_j) and the epoch of non-relativistic transition (t_{NR}) as inputs. The code then evaluates the afterglow flux at various time steps, which are also user specified, by evolving all the guess values at those epochs. The model flux thus estimated is then corrected for the total extinction (Galactic + host) and host flux contribution. The resultant flux is then compared with the observed data points and χ^2 is calculated. Minimum of the χ^2 distribution is

then searched using grid-search method and the corresponding parameters are returned as the best fit parameters. Apart from the above mentioned values the code can also fit for the extinction in the host galaxy.

Estimation of Physical Parameters : The multiband observations of GRB afterglows are important for characterising the afterglow spectrum. By using the multi-band light curves of the afterglows and by fitting an afterglow model using the above mentioned codes, one can determine the break frequencies and the peak of the spectrum along with other parameters. The evolution of the spectral breaks is intimately related to the physical situations prevailing at the radiating material as well as to the evolution of the shock-wave. Wijers and Galama (1999) and Chevalier and Li (2000) provide a quantitative description of the spectral breaks in terms of the physical parameters such as ϵ_e, ϵ_B, energy of the explosion and the density of circum-burst medium (see Chapter 1 for detailed description of the physical parameters). We have used this formulation to estimate the physical parameters of the fireball. Bhattacharya (2001) generalises these formulations to the cases where $1.0 < p < 2.0$. We have also used the expression from Bhattacharya (2001) to estimated the physical parameters in cases where $1.0 < p < 2.0$.

In most of the cases, the afterglow is too weak to be detected in the radio wavebands. The self-absorption frequency (ν_a), which has a strong dependence on the density of the circum-burst medium, normally lies in the radio-millimeter waveband. The non-detection of the radio afterglow then leaves us short of one parameter to determine the physical parameters. In such situations, we have expressed the physical parameters in terms of the rest three spectral parameters (viz. ν_m, ν_c, F_{peak}) and the density of the circum-burst medium. As an additional constraint, in such situations, we assume either the energy

equipartition between the accelerated electrons and the magnetic field i.e. $\epsilon_e = \epsilon_B$ or $\epsilon_e = \sqrt{\epsilon_B}$. The later situation has been proposed by Medvedev (2006) as a more likely situation for the GRB fireballs.

Double Jet : Some of the afterglows have been explained as being due to two physically distinct jets, instead of usual one. To take this into account, we have generalised our above mentioned code. The code calculates flux contributions from both the jets and corrects them for extinction and host contribution in a similar way as mentioned above. It then adds the fluxes so calculated before comparing with the observed data points. Best fit parameters are estimated and returned in a similar way as in the case of single jet above. This code was used for estimating the best fits to the afterglow of GRB 050401 described in Chapter 5.

The best fit parameters obtained using this code for various data sets are discussed in Chapter 4, Chapter 5, Chapter 6. We have also plotted the resultant light curves generated using the best fit parameters in these chapters.

2.4 Summary

To summarize, we have briefly discussed the importance of multiband observations of GRB afterglows. We also explained, a computer code that we have developed to calculate multiband light curves as would be expected from a GRB afterglow by properly taking account various effects such as interstellar extintion, flux contribution from the host galaxy, evolution due to the lateral spreading of relativistic collimated outflows and also due to non-relativistic expansion of the outflow. The code smoothens the breaks, as would be expected to be seen, before comparing the model flux thus estimated with the observations.

Bibliography

Bhattacharya D. Bulletin of the Astronomical Society of India, 29, 107 (2001).

Calzetti D., Kinney A.L. and Storchi-Bergmann T. ApJ, 429, 582 (1994).

Chevalier R.A. and Li Z.Y. ApJ, 536, 195 (2000).

Frail D.A., Soderberg A.M., Kulkarni S.R. et al. ApJ, 619, 994 (2005).

Granot J. and Sari R. ApJ, 568, 820 (2002).

Massarotti M., Iovino A., Buzzoni A. and Valls-Gabaud D. A&A, 380, 425 (2001).

Mathis J.S. ARA&A, 28, 37 (1990).

Medvedev M.V. ApJ Lett, 651, L9 (2006).

Meszaros P. and Rees M.J. ApJ Lett, 418, L59+ (1993).

Rees M.J. and Meszaros P. MNRAS, 258, 41P (1992).

Resmi L., Ishwara-Chandra C.H., Castro-Tirado A.J. et al. A&A, 440, 477 (2005).

Sari R., Piran T. and Narayan R. ApJ Lett, 497, L17+ (1998).

Schlegel D.J., Finkbeiner D.P. and Davis M. ApJ, 500, 525 (1998).

Wijers R.A.M.J. and Galama T.J. ApJ, 523, 177 (1999).